Current Biology 20, 2052–2057, November 23, 2010 ©2010 Elsevier Ltd All rights reserved DOI 10.1016/j.cub.2010.10.025

Report

Synchronized Neural Input Shapes Stimulus Selectivity in a Collision-Detecting Neuron

Peter W. Jones[1] and Fabrizio Gabbiani[1,2,*]
[1]Department of Neuroscience, Baylor College of Medicine, One Baylor Plaza, Houston, TX 77030, USA
[2]Department of Computational and Applied Mathematics, Rice University, 6100 Main Street, Houston, TX 77005, USA

Summary

How higher-order sensory neurons generate complex selectivity from their simpler inputs is a fundamental question in neuroscience. The lobula giant movement detector (LGMD) is such a visual neuron in the locust *Schistocerca americana* that responds selectively to objects approaching on a collision course or their two-dimensional projections, looming stimuli [1–4]. To study how this selectivity arises, we designed an apparatus allowing us to stimulate, individually and independently, a sizable fraction of the ~15,000 elementary visual inputs impinging retinotopically onto the LGMD's dendritic fan [5–7] (Figure 1Ai). We then recorded intracellularly in vivo throughout the visual pathway, assessing the LGMD's activity and that of all three successive presynaptic stages conveying local excitatory inputs. Our results suggest that as collision becomes increasingly imminent, the strength of these inputs increases, whereas their latency decreases. This latency decrease favors summation of inputs activated sequentially throughout the looming sequence, making the neuron maximally sensitive to collision-bound trajectories. Thus, the LGMD's selectivity arises partially from presynaptic mechanisms that synchronize a large population of inputs during a looming stimulus and subsequent detection by postsynaptic mechanisms within the neuron itself. Analogous mechanisms are likely to underlie the tuning properties of visual neurons in other species as well.

Results

We took advantage of the fact that locusts possess apposition compound eyes, and thus the photoreceptors within each ommatidium (facet) comprise a single functional unit [8]. We designed a custom microscope to deliver independent focal stimulation to ~300 facets on the eye (see Figure S1 available online). This allowed us to control ~5% of the excitatory synaptic inputs to the lobula giant movement detector (LGMD) while maintaining the ability to record intracellularly from neurons of the excitatory pathway in vivo. Additionally, this apparatus also allowed us to decompose looming stimuli into their elementary visual components, due to the discrete sampling inherent to the ommatidial eye lattice. We verified individual facet stimulation on the eye by mapping the receptive fields of single photoreceptors. A representative receptive field is shown overlaid on an image of the eye in Figure 1Biii, along with membrane potential traces from which it was generated (Figures 1Bi and 1Bii).

*Correspondence: gabbiani@bcm.edu

The logarithmic speed dependence of LGMD's excitation [9] suggests correlation-type interactions between retinotopic inputs having adjacent receptive fields (Figure 1Aii). In fact, a model of the LGMD endowed with such interactions reproduces several of its response characteristics [10]. Such mirror symmetric correlation detectors comprise the Reichardt model of motion detection in insects [11, 12], which is closely related to motion detection algorithms postulated in higher vertebrates [13]. Alternatively, the presynaptic inputs to the LGMD may act largely independently of each other (Figure 1Aiii) [4, 14]. Testing these hypotheses requires precise control over individual retinotopic inputs [11, 12], as achieved by our microscope.

LGMD responses to stimulation of individual facets showed a transient depolarization to brightness changes, with slightly stronger OFF than ON responses (mean = 8.4, 7.4 mV; standard error = 0.91, 0.81 mV; n = 22, 12 facets in 6 animals, respectively) [6]. Although this difference was not statistically significant ($p = 0.45$, t test), it may be amplified during the presentation of looming stimuli, when several thousand facets are activated. This may contribute to the stronger LGMD responses elicited by dark rather than bright looming stimuli [4]. To probe for the presence of correlation-type input to the LGMD, we delivered apparent motion stimuli consisting of ON or OFF light pulses with variable delays to two adjacent facets on the eye (Figures 1Ci–1Civ). The presence of correlator-type circuitry predicts a nonlinear response peak at an interstimulus interval matching the correlation detector's effective neural delay. We thus computed a summation index (SI; see Experimental Procedures) to identify responses higher than those expected from the sum of the two inputs delivered in isolation. No such nonlinear response increases could be found (Figure 1D), suggesting that no correlation mechanism exists within the LGMD's excitatory input. We also tested the directionality of apparent motion responses (Figure S1) because single correlation detectors are inherently directionally selective, and cells receiving correlation detector input often are as well [12, 15]. We found no evidence for direction selectivity, consistent with a lack of correlation detector input to the LGMD.

An alternative mechanism that could result in speed sensitivity of the LGMD's excitatory input is illustrated in Figure 2A. The faster the movement of a dark edge across a photoreceptor's receptive field (Figure 2Ai), the more rapidly the luminance encountered by the receptor will decrease (Figure 2Aii). If such luminance changes were faithfully transduced and the resulting response slopes extracted, it would yield a local signature of stimulus speed. To test this hypothesis, we presented edges drifting at speeds covering the dynamic range sensed by the LGMD neuron [9] and recorded single-photoreceptor responses. We found that the response slopes indeed correlated with edge speed (Figure 2B; $\rho = -0.86$, $p = 8.6 \times 10^{-22}$). Next, we designed single-facet stimuli consisting of luminance decreases (Figure 2C) and adjusted their duration to cover the range of photoreceptor response slopes elicited by moving edges. The slopes could be closely matched (Figure 2D), although the response transients were not exactly identical as a result of minor stimulus

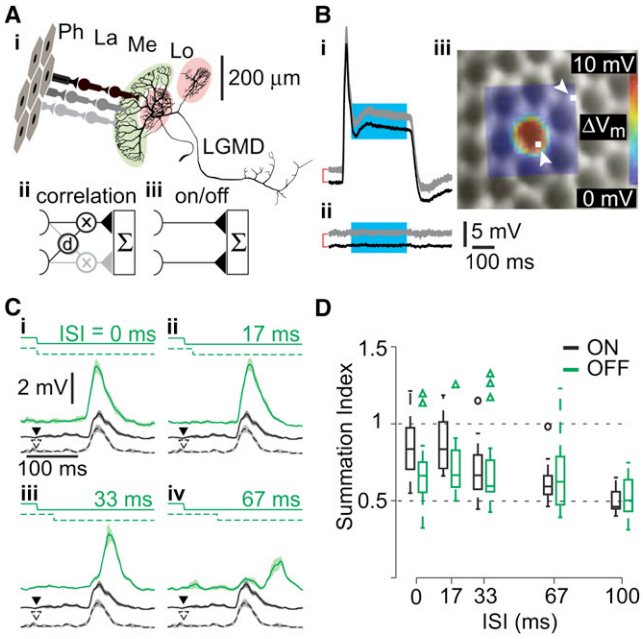

Figure 1. Probing Motion Detection Mechanisms via Visual Stimuli with Single-Facet Resolution

(Ai) Excitatory neural circuitry presynaptic to the lobula giant movement detector (LGMD). Photoreceptors (Ph), located within ommatidia (facets), synapse on cells in the lamina (La), which in turn contact medullary neurons (Me) that synapse onto the LGMD in the lobula (Lo). These inputs impinge on LGMD's large dendritic fan (highlighted in light green), while two separate dendritic fields receive inhibitory inputs (light red; scale bar applies to LGMD only).

(Aii and Aiii) The correlation diagram (Aii) illustrates hypothetical delay (d) and multiply (×) interactions between adjacent LGMD inputs (one input in black, the other gray), in contrast to independent input channels (Aiii). Both models include summation (Σ) in the LGMD.

(Bi and Bii) Single-photoreceptor responses (gray, n = 3 trials) and mean (black) to a 5 × 5 μm stimulus positioned on a visually identified ommatidium (Bi) and beside one (Bii). For clarity, the mean responses have been shifted vertically (red brackets, subsequent offsets left unmarked).

(Biii) Receptive field (RF) of a photoreceptor, mapped using a 20 × 20 location grid, superimposed on the simultaneously acquired microscopic image of the eye lattice. White squares, indicated by arrowheads, show the stimulation locations corresponding to the traces in (Bi) and (Bii). The RF was constructed by averaging over the cyan section of the traces in (Bi) and (Bii). The diameter of an ommatidium is ~25 μm.

(Ci–Civ) LGMD responses to apparent motion stimuli. Two adjacent facets were stimulated by a luminance step decrease with varying interstimulus intervals (ISIs; top solid and dashed lines). The LGMD response is illustrated below the stimulus in green (median filtered, mean response and standard error of the mean [SEM]; n = 9–10 trials). Responses to stimulation of each facet in isolation are shown as black solid and dashed lines (arrowheads indicate stimulus onset). Only OFF responses are shown.

(D) Distributions of summation indices as a function of ISI are shown as box plots, with ON responses in black and OFF responses in green (n = 26 facet pairs in 9 locusts). For each box, the central line indicates the median, the lower and upper boundaries are the 25th and 75th percentiles, and the whiskers indicate the extent of the data (outliers marked by circles and triangles, respectively).

brightness and stimulation protocol differences (Figure S2). Recordings from large monopolar cells (LMCs) in the lamina, which are most likely the next stage of the visual pathway [16], revealed that these neurons responded with increasing depolarization as the slope of the photoreceptor response became more negative (Figure 2E). Thus, our results establish that in the locust, these neurons effectively extract the slope of the photoreceptor response, consistent with the high-pass filtering properties reported in other insect species [17, 18]. Importantly, we also found that the delay of the peak response decreased as the stimulus duration became shorter. Because recording from the transmedullary neurons that synapse onto the LGMD is not yet technically feasible, we probed that stage of the excitatory pathway by voltage clamping the LGMD. We could successfully resolve excitatory postsynaptic currents elicited by single-facet stimulation and found that their strength and latency also depended on the time course of the associated luminance change (Figure 2F). In current clamp, the LGMD's membrane potential depolarizations elicited by single-facet stimulation had similar properties, except for a broadening, presumably caused by the filtering associated with the neuron's membrane time constant (Figure 2G). Thus, the decrease in response latency was consistently maintained from the sensory periphery to the LGMD (Figure 2H). Remarkably, the strongest single-facet stimuli could reliably elicit a few spikes in the LGMD, which occurred with precise timing (Figure 2G). The mean difference in first-spike latency for all stimulus-induced spikes was 4.6 ms (standard deviation = 3.5 ms, n = 50 trials).

These results suggest a mechanism that could tune the LGMD neuron to looming stimuli. As illustrated in Figure 3A, if an object approaches on a collision course at constant velocity, v, the angular speed, θ', of its expanding edges increases nonlinearly with time because the subtended half-angle, θ, is given by $\tan\theta = l/vt$, where t is time to collision and l is the object's half-size [19]. This in turn will cause increasingly rapid luminance changes as facets are stimulated in quick succession (Figures 3Ai–3Aiii) and will tend to synchronize the resulting excitatory input impinging onto the LGMD (Figure 3Aiv). We tested this hypothesis by disrupting the orderly sequence of luminance changes over single facets, either by randomly shuffling their order of appearance or by keeping the duration of each luminance change constant (Figures 3Av and 3Avi). First, we tested the effect of shuffling the sequence on a local scale by selecting an array of 3 × 15 facets and stimulating them sequentially with increasingly fast luminance changes, mimicking a looming stimulus edge during expansion at fast, medium, or slow speeds. We recorded LGMD responses to these "pseudolooming" stimuli and compared them to responses to corresponding shuffled stimuli. Because these stimulus differences might also modulate feedforward inhibition [20], we performed these experiments after local application of the selective $GABA_A$ antagonist picrotoxin to isolate the excitatory input to the LGMD. As illustrated in Figure 3C, we observed that the peak firing rates elicited in response to pseudolooming stimuli were larger than in the corresponding shuffled conditions. In a subset of neurons, we also obtained intracellular recordings, which showed a similar attenuation of the peak membrane potential.

To further test this synchronization hypothesis on a larger and behaviorally relevant spatial scale [21, 22], we used a monitor for visual stimulation at the expense of the ability for precise, single-facet stimulation. We designed a "coarse" looming stimulus by discretizing visual space within 3° × 3° regions, approximately of the same size as single photoreceptors' receptive fields [23]. During a coarse loom, the time course of the luminance change in each of these "pixels" matched that elicited by a looming stimulus, integrated over the pixel's area. As expected from the fact that this discretization matched the spatial resolution of the locust

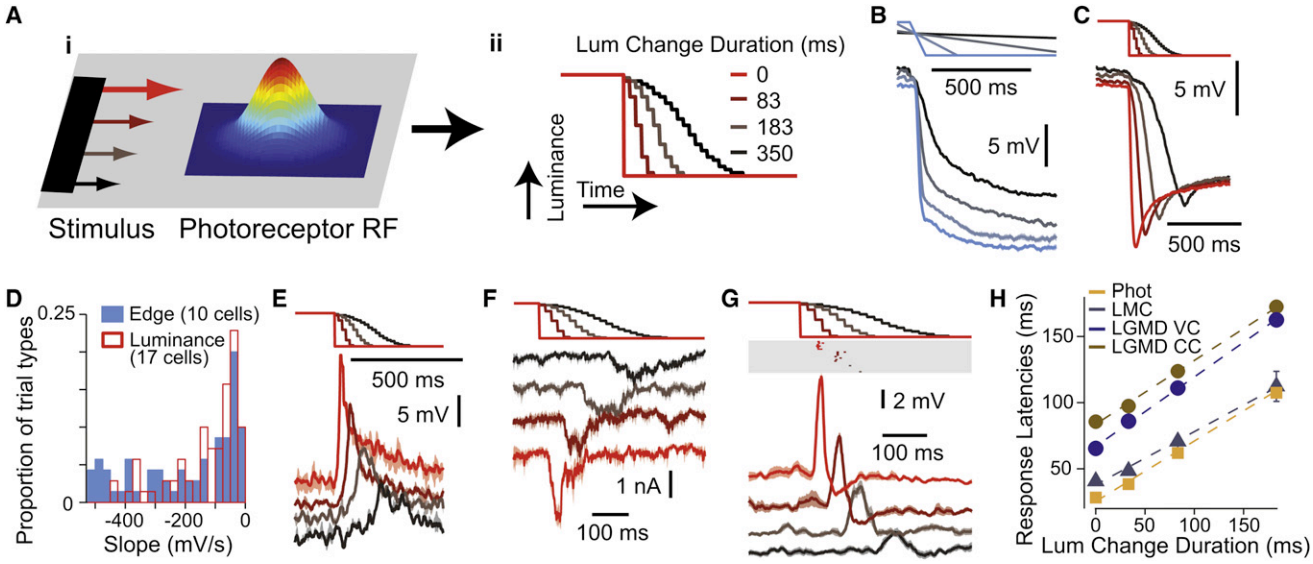

Figure 2. Single-Facet Signaling of Stimulus Speed

(Ai and Aii) Model of velocity encoding by single photoreceptors. As a dark object crosses the Gaussian-shaped receptive field (Ai), it produces a luminance (Lum) change whose duration depends on stimulus speed (Aii). Luminance change durations are those employed in (C) and (E)–(G). Luminance steps occur at the refresh rate of the display.

(B) Photoreceptor response to a translating dark edge moving at various speeds (20°/s, 80°/s, 319°/s, and 1275°/s). Top lines show edge position over time (maximal displacement 102°). Lines at bottom are mean responses with SEM envelopes (n = 8 trials).

(C) Photoreceptor responses to single-facet microscopic luminance modulation. The top stimulus traces show the luminance change over time, and the correspondingly colored traces below show the resulting photoreceptor responses.

(D) Distribution of photoreceptor response slopes (calculated from 20% to 80% of the peak response) evoked by edge motion (blue; 20°/s–1275°/s, contrast = 0.96; 10 cells) and single-facet luminance changes (red, outlined; transition duration = 1–517 ms; 17 cells).

(E) Large monopolar cell (LMC) responses to luminance changes similar to those in (C) (n = 2–4 trials).

(F) LGMD responses (I_m) to single-facet luminance changes under voltage clamp (VC) at close to resting potential (−64 mV, n = 5 trials).

(G) LGMD responses to single-facet luminance changes under current clamp (CC). The membrane potential (V_m) traces at the bottom have been median filtered to remove spikes prior to averaging (n = 6–7 trials). The rasters above report the timing of those spikes.

(H) Peak LGMD and LMC response times and photoreceptor response onset time (20% of peak) as a function of luminance change duration. Dashed lines show least-squares linear fits, with slopes of 0.46, 0.40, 0.52, and 0.49 and intercepts of 25, 37, 66, and 84 ms for photoreceptors, LMCs, and the LGMD (I_m and V_m), respectively. The 95% confidence intervals on the fitted slopes were ±0.01, ±0.08, ±0.06, and ±0.08. Error bars denote SEM (photoreceptors, n = 91–100 trials; LMCs, n = 39–42; LGMD VC, n = 115–121; LGMD CC, n = 133–137).

compound eye, responses to coarse looming stimuli were similar to those elicited by conventional looming stimuli (Figure S3). To disrupt the synchronization of individual inputs impinging onto the LGMD, we adopted the strategy illustrated in Figure 3Avi. Namely, we fixed the luminance change time course of all individual pixels to the average of the coarse stimulus and adjusted their onset times so as to closely reproduce the whole-screen luminance time course of the looming stimulus (Figure S4). We denote these stimuli by "constant-rate" looming stimuli because the rate of luminance change is fixed over time. In Figure 4, we compare the LGMD responses to the coarse looming stimuli with those elicited by constant-rate looming stimuli, for three values of the stimulus-size-to-speed ratio, $l/|v|$, characterizing the time course of the approach angle. As can be seen from both the single-neuron spike trains (Figure 4A) and the population averages, constant-rate looming stimuli evoked much-attenuated responses compared to coarse looming, when measured by either the peak firing rate or the spike count (Figures 4B and 4C). Additionally, the timing of the response peak, which signals an angular threshold size that is behaviorally relevant for collision avoidance behaviors [24, 25], was disrupted for the constant-rate looms. Specifically, response peaks occurred earlier relative to collision time for constant-rate stimuli (Figure 4D), causing angular threshold sizes [19] to change from 21.2° for coarse looming to 9.8° for constant rate.

Discussion

These results suggest that synchronization of the excitatory synaptic inputs impinging onto the LGMD's fan-shaped dendrite indeed plays an important role in tuning the neuron to looming stimuli. In this pathway, synchronization arises through a decrease in the latency of excitatory inputs as the instantaneous angular speed of the edges sweeping across individual photoreceptor receptive fields increases. Edge acceleration is in turn a defining feature of looming stimuli, entailing specificity to this mechanism. Although edge acceleration had previously been recognized as important for sustained LGMD responses [4, 26] and several mechanisms capable of reducing responses to its nonpreferred stimuli had been identified [20, 26–28], no mechanism specifically facilitating responses to accelerating or looming stimuli was known.

The synchronization mechanism unveiled by our experiments appears to rely chiefly on the temporal coherence of signals across individual facets. Indeed, we found no evidence for correlation-type motion detection circuitry that would enhance responses to the spatiotemporal coherence of a stimulus on a fine scale, across adjacent facets. However, our

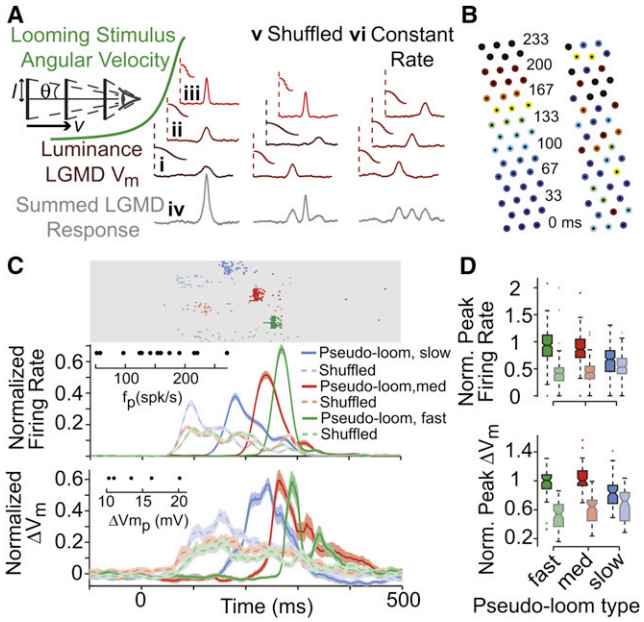

Figure 3. Temporal Synchronization of LGMD Excitation by Accelerating Sequences of Luminance Changes

(Ai–Aiv) Temporal synchronization hypothesis and tests. The accelerating angular velocity of a looming stimulus (green) stimulates successive facets with increasingly rapid changes in luminance, leading to decreasing response latencies (Ai–Aiii; luminance/response pairs connected by vertical dashed lines). This sequence synchronizes excitatory inputs, resulting in strong LGMD responses (Aiv).

(Av and Avi) Shuffled (Av) and constant-rate (Avi) columns show stimulus manipulations used to disrupt this synchronization, by either shuffling the order of presentation or keeping the rates of single-facet luminance changes constant. *l*, stimulus half-size; *v*, approach velocity; θ, half-angle subtended at the eye.

(B) Stimulus positions used to independently target 45 facets in a pseudo-looming experiment. The numbers denote the luminance change onset times (in milliseconds) for alternate rows of facets; the color indicates its duration from long (cold colors) to short (hot colors; black is an instantaneous change). Left array shows pseudolooming, with a coherent activation sequence from bottom to top (slow pseudoloom condition); right array is corresponding shuffled condition.

(C) LGMD responses to three pseudolooms (slow, medium, and fast) and the corresponding shuffled stimuli. The top rasters (light-gray area) show spiking responses in one representative experiment. The traces below show normalized instantaneous firing rates (spike trains convolved with a Gaussian filter; σ = 20 ms), for the recorded sample of LGMD neurons (16 animals, n = 187–202 trials per condition). For each animal, single-trial responses were normalized to the maximum, trial-averaged peak firing rate. The bottom traces show the normalized (as above), median-filtered membrane potential in the subset of neurons for which we obtained intracellular recordings (5 animals, n = 45–49 trials per condition). All traces and envelopes indicate mean and SEM. Insets show the distribution of peak firing rate (f_p) and membrane potential change (ΔVm_p) values used for normalization.

(D) Box plots showing the distributions of normalized peak firing rates and normalized peak membrane potential changes. Pseudolooming/shuffled pairs of all types have significantly different median peak firing rates ($p_{RS} < 10^{-4}$) and peak membrane potential changes ($p_{RS} < 0.003$), as indicated by nonoverlapping notches in box plots.

results do not rule out that the spatial coherence of looming stimuli may also contribute to the looming sensitivity of the LGMD. For example, excitatory or inhibitory input strength could be modulated by spatiotemporal coherence at larger scales than that detected by correlation of signals across adjacent facets.

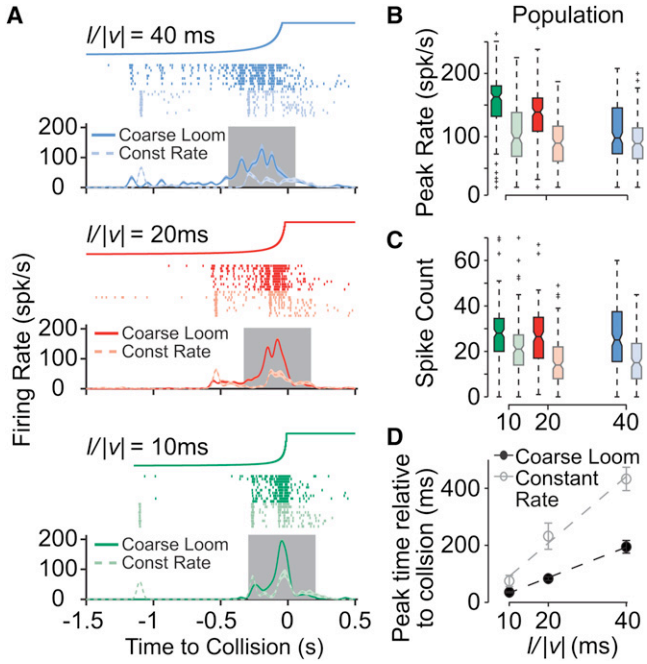

Figure 4. LGMD Responses to Modified Looming Stimuli

(A) LGMD responses to "coarse" and "constant-rate" looming stimuli in a representative single experiment. Top traces show the stimulus angular size over time of the corresponding looming stimulus (final full angle = 85°). Rasters show LGMD spikes in each trial for coarse (saturated color) and constant-rate (lighter color) looming stimuli. Correspondingly colored traces below show mean firing rates. Gray area indicates the 500 ms window centered on the LGMD peak firing rate in which spike counts were tabulated.

(B and C) Box plots, formatted and colored as in Figure 3, showing the distributions of peak firing rates and spike counts for all trials pooled across the population of experiments (12 animals, n = 118–122 trials per condition). Looming stimulus type had a significant effect on the peak firing rate, and the firing rates for constant-rate looming were significantly lower than those for coarse looming for all *l*/|*v*| values ($p_{KW} = 10^{-20}$–10^{-5}, $p_{HSD} < 0.05$).

(D) Timing of the peak firing rate as a function of *l*/|*v*| for coarse (black) and constant-rate (gray) looming stimuli. Plotted circles are population mean times, with error bars indicating SEM. Dashed lines show linear fits to the data, with slopes of 5.3 and 11.7 and intercepts of −20 and −19 ms for looming and constant-rate stimuli, respectively.

Both experimental and theoretical arguments have implicated synchronization of synaptic input in the tuning of mammalian visual neurons [29–31], suggesting that analogous mechanisms may be at work. The postsynaptic detection of such neural synchrony could be based on the spatial specificity of synaptic inputs [32] in the locust visual system [6] and in other species ([33], but see [34]). Our results show that the systematic mapping of individual presynaptic neural components within well-defined neural circuits is a powerful tool to explain how the complex tuning properties of higher-order neurons arise in vivo.

Experimental Procedures

Animal Dissection and Electrophysiology

Locusts were mounted in a plastic holder and dissected as previously described [35]. Sharp microelectrodes were used for intracellular recordings from photoreceptors, LMCs (80–240 MΩ, 2 M KAc/0.5 M KCl), and the LGMD (8–30 MΩ, 2 M KAc/0.5 M KCl or 3 M KCl for voltage clamp). Intracellular signals were low-pass filtered (V_m = 10 kHz, I_m = 5 kHz) and digitized (20 kHz). Photoreceptor and LGMD recordings used borosilicate electrodes (1.2/0.8 mm and 1.2/0.5 OD/ID, respectively; WPI), whereas LMC recordings used aluminosilicate (1.0 OD; Harvard Apparatus). An Ag/AgCl wire was

used as reference. Current-clamp recordings were made in discontinuous current clamp (DCC, ~25 kHz switching frequency) or bridge mode. Voltage-clamp recordings from the LGMD used discontinuous single-electrode voltage clamp (dSEVC, ~25 kHz switching amplifier; NPI). All dSEVC electrodes had <20 MΩ resistances, and electrode resistance (bridge) or capacitance (DCC/dSEVC) was fully compensated in the bath immediately prior to tissue penetration. Intracellular recordings were obtained from the lobula and lamina through the desheathed optic lobe and from the retina through a small (~50 × 50 μm) hole just below the dorsal rim of the eye. Photoreceptor recordings were identified by their resting potential (~ −50 mV) and depolarizing responses to luminance increases. The extracellular potential of the lamina modulates in phase with a flashing light stimulus, allowing identification of LMCs by a slight resting hyperpolarization and transient, antiphase responses to light flashes. LGMD recordings were identified by the cell's 1:1 spike correspondence with the simultaneously recorded descending contralateral movement detector (DCMD) neuron [36]. The cell was penetrated in the proximal region of the excitatory dendritic field, with spike heights varying between 20 and 50 mV. Stable LGMD recordings could be maintained for typically >60 min. Extracellular signals were acquired as previously described. DCMD spikes were detected by thresholding, and instantaneous firing rates were calculated by convolving individual spike trains with a Gaussian window (σ = 20 ms).

Injection of PCTX in the Lobula

Prior to pseudolooming experiments, small volumes of picrotoxin (PCTX, 10 mM) in aqueous solution were injected into the lobula to block feedforward inhibition onto the LGMD [21]. Fast green (0.5%) was used for injection visualization. The injection pipettes had tip diameters of ~2 μm and were visually positioned against the posterior dorsal aspect of the lobula using a micromanipulator, close enough that the injections penetrated the tissue. PCTX acted quickly (<1 min), with LGMD responses to visual stimuli increasing markedly. Only the lobula was stained by the injection, making it unlikely that the medulla or lamina neuropils (located several hundred micrometers away) were affected. Additionally, the pipettes were placed into the bath only immediately before injection and were removed immediately after, and the saline was exchanged to prevent diffusion through the bath to other brain areas.

Visual Stimulation

Visual stimuli were generated using custom software on a PC running a real-time operating system (QNX 4). Wide-field dark (2 cd/m^2) and bright (90 cd/m^2) stimuli were presented on a CRT monitor (200 Hz). Single-ommatidium-resolution stimulation was achieved by projecting an image generated using a DLP projector (NEC LT140) through a custom-built microscope mounted horizontally on a vibration-isolated optical table (illuminance range = 4–2530 lux). Both displays were calibrated to ensure linear, 6-bit resolution control over light levels. Single-facet and pseudolooming experiments used a 20×/0.5 NA and a 10×/0.3 NA water-immersion objective, respectively. A watertight plastic cup was placed around the objective and sealed to the animal holder with silicone grease, and the animal's right eye was submerged in water (to neutralize the optical power of the facet lens) for imaging and stimulation. The focal plane was set behind the cornea.

Single-Facet and Apparent Motion Stimuli

Each stimulus spot was 2 × 2 pixels (5 × 5 μm) in size, positioned in the center of each ommatidium. Each stimulus was a 1500 ms light pulse from baseline (4 lux) to a variable maximum (≤2530 lux). Luminance changes had the time course of a cumulative Gaussian, with their mean and two standard deviations equal to half the transition duration. Multiple facets or adjacent facet pairs were stimulated when recording from the LGMD (four maximum, spaced with at least two intermediate facets). Each facet was stimulated less than once per minute to avoid local habituation. Stimuli were presented every 5 s for LMC and photoreceptor experiments. Trial types within all experiments were pseudorandomly interleaved.

Pseudolooming Stimuli

The stimuli spanned three facet rows, each 15 facets long, with each stimulus point positioned over a single facet. The stimulus points along each row were illuminated in sequence, with the onsets of luminance changes one frame (1/60 s) apart, over a period of 233 ms (Figure S4). The duration of luminance changes for single facets was chosen to span the range to which the LGMD is sensitive and progress through that range at different rates. The progression of luminance changes was chosen to mimic the acceleration caused by a looming edge; the constant interval between stimulus point onsets allowed for a dissociation of stimulus progression across the retina (number of facets stimulated over a period of time) and luminance change at single points, which is not possible using an actual moving edge. The shuffled condition pseudorandomly reassigned the time course of luminance changes across stimulus points, with the constraint that for each frame, the mean duration of luminance changes for the three stimulated facets must lie within 20%–80% of the range of luminance change durations. This condition prevented the fastest luminance changes from occurring simultaneously, as in the pseudolooming stimuli. In every experiment, each facet was stimulated individually to confirm that there was no positional bias in response strength that could cause a difference between pseudolooming and shuffled conditions. Stimuli were presented every 40 s.

Constant-Rate Looming

To construct the "constant-rate" looming stimuli, we first created a looming stimulus with a spatial resolution matching that of the locust eye (3° × 3° pixels, 729 pixels total, covering 85° × 85°). In this stimulus (coarse looming), each pixel's luminance follows the same time course as the luminance of the simulated approaching object integrated over its area. To create the constant-rate loom, we constrained the luminance change of each pixel to have a duration equal to the mean across pixels during the coarse loom. We then adjusted each pixel's luminance change onset time to match the temporal profile of the whole-screen luminance during the normal looming stimulus. Stimuli were presented once per minute.

Data Analysis and Statistics

Data analysis was carried out with custom MATLAB programs (MathWorks). The nonparametric Wilcoxon rank-sum test (denoted p_{RS}) was employed for comparisons of two independent data sets for the pseudolooming experiments, whereas a Kruskal-Wallis test (p_{KW}) followed by Tukey's honestly significant difference test (p_{HSD}) was used for looming experiments where three conditions were compared. LGMD current clamp recordings were median filtered (8 ms window) for spike removal. Summation indices were calculated as $SI = R_{both}/(R_{facet1} + R_{facet2})$, with R being the peak of the median-filtered V_m traces.

Supplemental Information

Supplemental Information includes Supplemental Results and Discussion and four figures and can be found with this article online at doi:10.1016/j.cub.2010.10.025.

Acknowledgments

We would like to thank H. Krapp, J. Maunsell, H. Ogmen, P. Saggau, and S. Peron for comments. This work was supported by grants from the National Science Foundation and the National Institute of Mental Health.

Received: July 16, 2010
Revised: September 30, 2010
Accepted: October 12, 2010
Published online: November 4, 2010

References

1. Schlotterer, G.R. (1977). Response of the locust descending movement detector neuron to rapidly approaching and withdrawing visual stimuli. Can. J. Zool. *55*, 1372–1376.
2. Rind, F.C., and Simmons, P.J. (1992). Orthopteran DCMD neuron: a reevaluation of responses to moving objects. I. Selective responses to approaching objects. J. Neurophysiol. *68*, 1654–1666.
3. Hatsopoulos, N., Gabbiani, F., and Laurent, G. (1995). Elementary computation of object approach by wide-field visual neuron. Science *270*, 1000–1003.
4. Simmons, P.J., and Rind, F.C. (1992). Orthopteran DCMD neuron: a reevaluation of responses to moving objects. II. Critical cues for detecting approaching objects. J. Neurophysiol. *68*, 1667–1682.
5. Strausfeld, N.J., and Nässel, D.R. (1981). Neuroarchitectures serving compound eyes of crustacea and insects. In Comparative Physiology and Evolution of Vision of Invertebrates, B: Invertebrate Visual Centers and Behavior I, Handbook of Sensory Physiology, *Volume 7*, H. Autrum, ed. (Berlin: Springer-Verlag), pp. 1–132.

6. Peron, S.P., Jones, P.W., and Gabbiani, F. (2009). Precise subcellular input retinotopy and its computational consequences in an identified visual interneuron. Neuron *63*, 830–842.
7. Rind, F.C., and Simmons, P.J. (1998). Local circuit for the computation of object approach by an identified visual neuron in the locust. J. Comp. Neurol. *395*, 405–415.
8. Shaw, S.R. (1968). Organization of the locust retina. Symp. Zool. Soc. Lond. *23*, 135–163.
9. Krapp, H.G., and Gabbiani, F. (2005). Spatial distribution of inputs and local receptive field properties of a wide-field, looming sensitive neuron. J. Neurophysiol. *93*, 2240–2253.
10. Harrison, R.R. (2005). A biologically inspired analog IC for visual collision detection. IEEE Trans. Circuits Syst. *52*, 2308–2318.
11. Reichardt, W. (1987). Evaluation of optical motion information by movement detectors. J. Comp. Physiol. A Neuroethol. Sens. Neural Behav. Physiol. *161*, 533–547.
12. Single, S., Haag, J., and Borst, A. (1997). Dendritic computation of direction selectivity and gain control in visual interneurons. J. Neurosci. *17*, 6023–6030.
13. Bradley, D.C., and Goyal, M.S. (2008). Velocity computation in the primate visual system. Nat. Rev. Neurosci. *9*, 686–695.
14. Rowell, C.H., and O'Shea, M. (1976). The neuronal basis of a sensory analyser, the acridid movement detector system. I. Effects of simple incremental and decremental stimuli in light and dark adapted animals. J. Exp. Biol. *65*, 273–288.
15. Haag, J., and Borst, A. (2004). Neural mechanism underlying complex receptive field properties of motion-sensitive interneurons. Nat. Neurosci. *7*, 628–634.
16. James, A.C., and Osorio, D. (1996). Characterisation of columnar neurons and visual signal processing in the medulla of the locust optic lobe by system identification techniques. J. Comp. Physiol. A Neuroethol. Sens. Neural Behav. Physiol. *178*, 183–199.
17. Laughlin, S.B., and Hardie, R.C. (1978). Common strategies for light adaptation in the peripheral visual systems of fly and dragonfly. J. Comp. Physiol. *128*, 319–340.
18. Juusola, M., Uusitalo, R.O., and Weckström, M. (1995). Transfer of graded potentials at the photoreceptor-interneuron synapse. J. Gen. Physiol. *105*, 117–148.
19. Gabbiani, F., Krapp, H.G., and Laurent, G. (1999). Computation of object approach by a wide-field, motion-sensitive neuron. J. Neurosci. *19*, 1122–1141.
20. Gabbiani, F., Cohen, I., and Laurent, G. (2005). Time-dependent activation of feed-forward inhibition in a looming-sensitive neuron. J. Neurophysiol. *94*, 2150–2161.
21. Gabbiani, F., Krapp, H.G., Koch, C., and Laurent, G. (2002). Multiplicative computation in a visual neuron sensitive to looming. Nature *420*, 320–324.
22. Fotowat, H., and Gabbiani, F. (2007). Relationship between the phases of sensory and motor activity during a looming-evoked multistage escape behavior. J. Neurosci. *27*, 10047–10059.
23. Wilson, M. (1975). Angular sensitivity of light and dark adapted locust retinula cells. J. Comp. Physiol. *97*, 323–328.
24. Santer, R.D., Rind, F.C., Stafford, R., and Simmons, P.J. (2006). Role of an identified looming-sensitive neuron in triggering a flying locust's escape. J. Neurophysiol. *95*, 3391–3400.
25. Fotowat, H., Harrison, R.R., and Gabbiani, F. (2011). Multiplexing of motor information in the discharge of a collision detecting neuron during escape behaviors. Neuron, in press.
26. Peron, S., and Gabbiani, F. (2009). Spike frequency adaptation mediates looming stimulus selectivity in a collision-detecting neuron. Nat. Neurosci. *12*, 318–326.
27. O'Shea, M., and Rowell, C.H. (1975). Protection from habituation by lateral inhibition. Nature *254*, 53–55.
28. Zaretsky, M. (1982). Quantitative measurements of centrally and retinally generated saccadic suppression in a locust movement detector neurone. J. Physiol. *328*, 521–533.
29. Monier, C., Chavane, F., Baudot, P., Graham, L.J., and Frégnac, Y. (2003). Orientation and direction selectivity of synaptic inputs in visual cortical neurons: a diversity of combinations produces spike tuning. Neuron *37*, 663–680.
30. Priebe, N.J., and Ferster, D. (2005). Direction selectivity of excitation and inhibition in simple cells of the cat primary visual cortex. Neuron *45*, 133–145.
31. Wang, H.P., Spencer, D., Fellous, J.-M., and Sejnowski, T.J. (2010). Synchrony of thalamocortical inputs maximizes cortical reliability. Science *328*, 106–109.
32. Polsky, A., Mel, B.W., and Schiller, J. (2004). Computational subunits in thin dendrites of pyramidal cells. Nat. Neurosci. *7*, 621–627.
33. Bollmann, J.H., and Engert, F. (2009). Subcellular topography of visually driven dendritic activity in the vertebrate visual system. Neuron *61*, 895–905.
34. Jia, H., Rochefort, N.L., Chen, X., and Konnerth, A. (2010). Dendritic organization of sensory input to cortical neurons in vivo. Nature *464*, 1307–1312.
35. Peron, S.P., Krapp, H.G., and Gabbiani, F. (2007). Influence of electrotonic structure and synaptic mapping on the receptive field properties of a collision-detecting neuron. J. Neurophysiol. *97*, 159–177.
36. O'Shea, M., and Rowell, C.H. (1976). The neuronal basis of a sensory analyser, the acridid movement detector system. II. response decrement, convergence, and the nature of the excitatory afferents to the fan-like dendrites of the LGMD. J. Exp. Biol. *65*, 289–308.